Energy 194 (2020) 116873

Contents lists available at ScienceDirect

Energy

journal homepage: www.elsevier.com/locate/energy

Electrodeposition preparation and optimization of fan-shaped miniaturized radioisotope thermoelectric generator

Zhiheng Xu [a, b], Junqin Li [a], Xiaobin Tang [a, b, *], Yunpeng Liu [a, b], Tongxin Jiang [a], Zicheng Yuan [a], Kai Liu [a]

[a] Department of Nuclear Science and Technology, Nanjing University of Aeronautics and Astronautics, 29 General Road, Jiangning District, Nanjing, 211106, China

[b] Key Laboratory of Nuclear Technology Application and Radiation Protection in Astronautics (Nanjing University of Aeronautics and Astronautics), Ministry of Industry and Information Technology, 29 General Road, Jiangning District, Nanjing, 211106, China

ARTICLE INFO

Article history:
Received 26 July 2019
Received in revised form
23 December 2019
Accepted 28 December 2019
Available online 30 December 2019

Keywords:
Energy conversion
Bismuth telluride
Bismuth antimony telluride
Radioisotope thermoelectric generator
Electrodeposition

ABSTRACT

In view of the current energy demand for miniaturized equipment in extreme environmental fields, such as in deep space exploration. A new fan-shaped radioisotope thermoelectric generator is innovatively presented and designed. Thin-film thermoelectric materials used for miniaturized radioisotope thermoelectric generators are first prepared by electrochemical methods. The prepared fan-shaped radioisotope thermoelectric generator has a volume of 5.75 cm^3 and consists of 8 thermoelectric modules and 32 thermoelectric legs. The study finds that when a 1.5 W heat source is loaded, the temperature difference of the device is 54.8 K, the output voltage and the maximum output power is 174.88 mV and 333.20 nW, respectively. On this basis, the number and size of the modules are optimized by the finite element method. When the thermoelectric leg size is optimized to 9 × 2 mm^2 and the number of modules is 8, the maximum output power can be up to 369.02 nW. The corresponding experimental verification work is further developed and discussed. This work provides a novel solution for the energy supply problem of small-volume devices in extreme space environments.

1. Introduction

With progress on science and technology, many micro/nano-scale electronic devices, especially miniaturized detectors and sensors, are designed for extreme environments, such as aerospace. Therefore, the demand for electricity from these components has been ever more urgent. Radioisotope thermoelectric generators (RTGs) can directly convert the decay heat of isotope heat sources into electrical energy through the Seebeck effect of semiconductor materials [1–6]. In the past few decades, RTGs are a relatively mature technology for energy supply and are commonly used in harsh environments [7–10]. However, the existing drawbacks of RTGs have rendered it unsuitable a power source for miniaturized electronic devices. The previously applied RTGs are generally inefficient and heavy [11–13]. The efficiency of RTG is approximately 6%. If the efficiency is not high enough, a larger volume is required to meet different power system technology needs. Excessively high mass results in the low energy density of the device. In addition, for most small size and low power consumption devices, the size of the power supply is still large. For example, the multi-mission RTG (MMRTG) has a mass of 45 kg, a length of 66 cm, and a diameter of 63 cm [13]. Conventional thermoelectric energy conversion devices are difficult to achieve miniaturization. This restricts the development to some extent in practical applications. In view of the failure of existing large-volume RTG satisfy the power supply need of small-scale electronic devices for deep-space detection, it is necessary to study the integration and miniaturization of RTGs.

At present, there has been a lot of research focused on miniaturization. Hi-z Corporation of the United States has also prepared and tested many small-volume TE devices, one of which contains 18 × 18 TE legs and has a volume of 22.9 × 0.38 × 0.38 mm^3 [14]. In 2006, J. Weber et al. have designed and fabricated a coiled-up TE micro power generator with a power density of 2 μW/cm^3 at 5 K temperature difference, which can be prepared to grow 1.8 m long

* Corresponding author. Department of Nuclear Science and Technology, Nanjing University of Aeronautics and Astronautics, 29 General Road, Jiangning District, Nanjing, 211106, China.
E-mail address: tangxiaobin@nuaa.edu.cn (X. Tang).

https://doi.org/10.1016/j.energy.2019.116873
0360-5442/

Nomenclature

Abbreviations

RTG	Radioisotope thermoelectric generator
MMRTG	Multi-mission radioisotope thermoelectric generator
TE	Thermoelectric
DC	Direct current

Symbols

Voc Open circuit voltage	
ΔTTE	Temperature difference
N	The number of TE legs
SA	Seebeck coefficient of the n-type TE materials
SB	Seebeck coefficient of the p-type TE materials
R	Internal resistance
L	The length of the TE leg
W	The width of the TE leg
S	The cross-sectional area of the TE leg
P_{out}	Output power
P_{in}	Input power
η	Energy conversion efficiency

strip, several μm thickness and 10 mm width [15]. S. A. Whalen et al. in 2008 prepared a small-sized RTG that was a volume of 4.3 cm^3, contains 11 pairs of thermoelectric (TE) legs, and can generate 450 μW of power output [16]. V. V. Gusev et al. in 2011 prepared a small-volume RTG-400 with an overall size of diameter × height = 10 cm × 11 cm, a mass of 0.6 kg, and an output power of 0.43 W [17]. In 2015, K. Uda et al. prepared a π-structured RTG with an open circuit voltage of 17.6 mV and an output power of 0.96 μW, which was consisted of 8 arrays and each consisting of 110 thermoelectric units [18]. In 2017, F. Suarez et al. fabricated a tiny RTG using bulk TE materials and liquid metal electrodes, which contains 64 TE legs and has an area of 4 cm^2 and a height of 0.64 mm [19]. In 2018, K. Liu et al. produced a high-performance radial RTG based on concentric filament architecture. The fabricated arrayed TE device with a dimension of 40 × 40 × 30 mm^3 can export 84.5 mV and 42.5 μW at the hot surface temperature of 398.15 K [20]. Z. C. Yuan et al. used screen-printing technique to prepare a flexible RTG with radial structure, which has an open-circuit voltage of 68.41 mV and an output power of 5.81 μW. The device consists of 5 pairs of TE legs with a diameter of 1.5 cm and an area of 1.77 cm^2 [21]. Y. C. Wang et al. prepared a novel wearable thermoelectric generator with the overall dimensions of 43.5 × 26.5 × 2.6 mm^3, an open-circuit voltage of 37.2 mV and the corresponding output power of 192.6 μW can be generated, when the temperature difference is 50 K [22]. E. Z. Mu et al. fabricated micro/nano-scale thermoelectric module with an effective working area of 11 mm^2, the thickness was about 1 μm, and the output power density could reach up to 2.9 × 10^5 W/m^3 [23]. In 2019, S. Lee et al. used silicon nanowires to make the thermoelectric device with a size of 1 × 1 cm^2, and the maximum power was 3.74 μW when the temperature difference is 180 K [24]. The intermixed bacterial nanocellulose and carbon nanotube fibers were also being tried to make flexible thermoelectric paper to reduce thermal conductivity and increase electrical conductivity [25]. Furthermore, thermoelectric devices based on hybrid energy conversion mechanisms have also been developed and explored [26–28].

The preparation method of TE materials considerably influences the performance of the device. At present, the conventional bulk TE preparation mainly adopts high-temperature sintering, and requires operating conditions such as high temperature and high pressure, which makes it difficult to precisely control the composition ratio of the material [29]. Moreover, bulk materials are difficult to apply in miniaturized devices, thereby limiting the integration advantages of the devices. Typical film formation methods, such as magnetron sputtering [30], and chemical vapor deposition [31,32] are expensive. This electrochemical method can be operated at room temperature and pressure environment, with lower cost and simpler operation, which is beneficial to industrial applications. The composition and properties of the material can also be precisely controlled by changing parameters such as deposition potential and electrolyte composition [33–36]. In this work, the flexible TE thin film materials were prepared using electrodeposition, and applied for the preparation of miniaturized RTG. The size and number of RTG modules were also optimized by simulation and experimentation, providing a viable candidate for future new energy supply systems.

2. Material and methods

2.1. Material preparation and device structure

Fig. 1 shows the schematic diagram of a fan-shaped RTG. The cylindrical radioisotope heat source is located at the center, surrounded by multiple TE modules, and the TE module is only a few tens of micrometers thick. In theory, the RTG can stack hundreds of modules in series. The TE module and its inter-layer series structure are shown in Fig. 1a. The TE module contains several pairs of p-n junctions and a flexible polyimide substrate that supports the film material. Polyimide materials have excellent high-temperature resistance, flexibility, and radiation resistance. The high-temperature resistance can ensure that the substrate is almost unaffected during the annealing process. The flexibility of the substrate can increase the bending strength and performance stability of the device itself. The anti-irradiation performance can meet the requirement for the space application. High-energy rays in the space will shorten the service life of the device, and the radiation-resistant polyimide substrate material can improve this situation.

The TE thin film material was prepared through pulse voltage electrodeposition, which adopts a three-electrode system. The working electrode is stainless steel, the counter electrode is a platinum plate, and the reference electrode is 3 M Ag/AgCl. The electrolyte solution was prepared using analytical reagents and deionized water. The main chemical reagents involved were $Bi(NO_3)_3 \cdot 5H_2O$, TeO_2, Sb_2O_3, and HNO_3, and the corresponding method has been elaborated in previous work [37]. The thickness of the stainless steel is 20 μm, and the effective area of the working electrode for material test is 1.5 × 1.5 cm^2 and for device preparation is 4 × 4 cm^2.

The preparation process of the fan-shaped flexible film RTG is shown in Fig. 2. The specific steps are as follows: (a) First, the TE film material was electrochemically deposited on the stainless steel substrate. (b) The high-temperature polyimide tape was affixed to the stainless steel substrate and (c) its surface was gently pressed with a finger to enhance the adhesion and allow the TE material to be slowly peeled off. Then the complete TE leg arrays were transferred to the polyimide substrate, and (d) the n-type and p-type TE leg arrays were obtained. (e) The film material was then placed into a vacuum tube furnace for annealing. The TE legs were assembled in series into a single TE module by using conductive silver paste as an electrode. (f) The TE modules were connected in series to form an RTG, which consists of eight TE modules each containing four TE legs with 11 mm length, 2 mm width, and 2–10 μm thickness. The

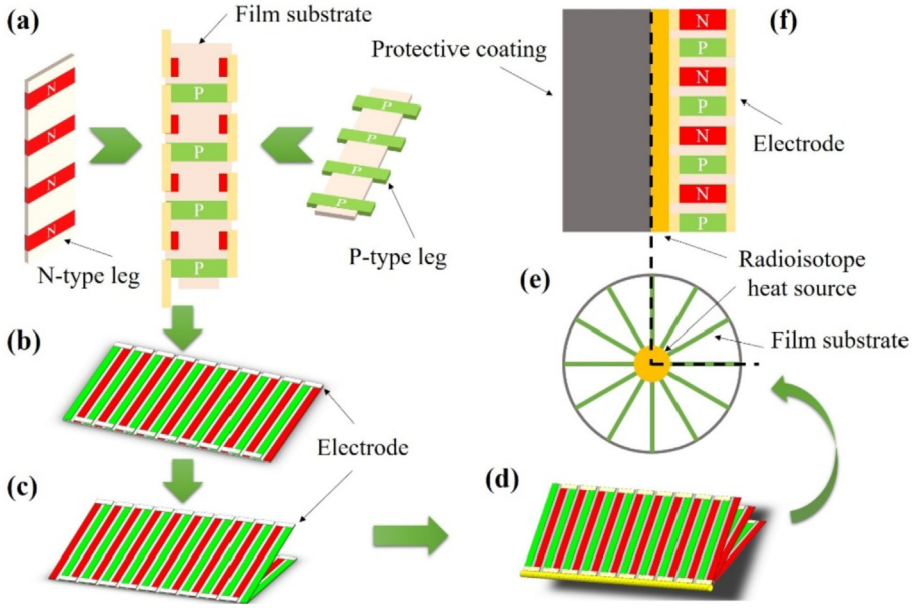

Fig. 1. Schematic diagram of RTG: (a) series connection diagram of thermoelectric modules; 3D stereo view of a (b) single module, (c) two modules and (d) three modules; (e) top view and (f) side view of RTG.

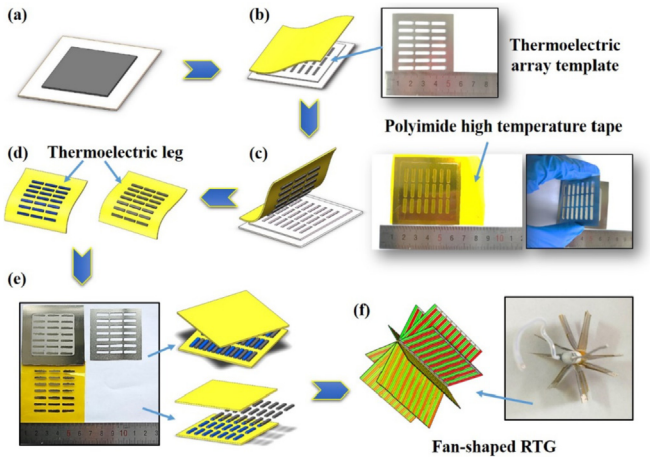

Fig. 2. RTG preparation: (a) deposition material; (b) bonded high temperature tape polyimide; (c) slowly strip the tape to get a complete array of TE legs; (d) n-type and p-type TE leg array; (e) assemble the TE leg arrays in series into a single TE module; (f) assemble multiple TE modules in series into a RTG.

overall size of the final device is approximately 5.7 cm^3, with a diameter of 25.8 mm.

2.2. Performance testing and parameter setting

During the output performance test, the heat source rod was inserted vertically in the center of the small RTG. A heat insulating material (1260 type aluminum silicate cotton with thermal conductivity of 0.03 W/m·K) was filled between the heat source and the TE module to prevent heat loss. Joule heat was used to simulate the decay energy of the radioactive fuel pellet. The programmable linear DC power supply (DP832A, RIGOL Technologies Inc.) can supply the heat source rod power, and which can have an equivalent heat source power of 0–1.5 W. J-type thermocouples were placed at the hot and cold ends of the RTG to measure the real-time temperature. The KTEI program controls the Keithley SourceMeter 4200 (Keithley 4200-SCS) to measure the electrical output performance of the RTG.

The open circuit voltage (V_{oc}) is the maximum output voltage of the TE module, which is proportional to the temperature difference (ΔT_{TE}) between the hot and cold ends of the TE leg, as shown in Equation (1).

$$V_{oc} = (S_B - S_A) \times \Delta T_{TE} \times n \tag{1}$$

Where n is the number of TE legs, and S_A and S_B are the Seebeck coefficient of the n-type and p-type TE materials, respectively. The internal resistance (r) of the device can be expressed as

$$r = \frac{2\rho l}{s} \times n \tag{2}$$

where l and s are the length and cross-sectional area of the TE leg, respectively. The output power (P_{out}) and the energy conversion efficiency (η) can be expressed respectively as

$$P_{out} = V \times I = \frac{V^2}{(R+r)^2} \times R \tag{3}$$

$$\eta = \frac{P_{out}}{P_{in}} \tag{4}$$

where R is the external load resistance of the device, P_{in} is the input power, such as the heat source power of the RTG. When $R = r$, the RTG exhibits the maximum output power P_{max} and conversion efficiency η_{max}. Depending on these formulas, the output performance of the TE device can be improved by optimizing the size parameters, such as the length l and cross-sectional area s of the TE leg. In addition, the internal resistance of the device is further strongly affected by the size parameters. Therefore, parameter optimization of the RTGs can improve performance output and power density to a large extent.

With regard to the thickness of the TE film material prepared by the experiment being in micro dimension, the material thickness setting during simulation was unmodified, and only the length l

and the width w of the TE leg were changed. According to the experimentally prepared TE leg size parameters l = 11 mm, w = 2 mm, the ranges of TE leg length l and width w during simulation were 1–22 mm and 0–3 mm, respectively, and the thickness was set to 5 μm. During the experiment, the size parameters of the heat source rod remained constant, with a diameter of 3.8 mm, a height of 2.5 cm, and a volume of 0.283 cm^3. The output performance of RTG with different TE leg size parameters was simulated and studied, when the loaded heat source power was set to 0–1.5 W.

In addition to the TE leg itself, the number will also have an impact on the output voltage and power. There is an optimal numerical period for specific application requirements. In the optimization design work, the number of five types of modules was set to 2, 4, 6, 8, and 10, and the TE leg size was fixed as 9 × 2 mm^2. Applied heat source power varied between 0.25 W and 1.5 W with an interval of 0.25 W for the three TE devices with the same volume and surface area. This simulation calculation can explore the effect of the number of TE modules on the output performance of the device. The small RTG provides an optimized design concept for the practical application of micro RTGs.

3. Results and discussion

3.1. Properties of n-type Bi_2Te_3 and p-type $Bi_{0.5}Sb_{1.5}Te_3$ thin films

Table 1 summarizes the performance of the n-type and p-type TE thin film materials deposited after annealing. Detailed material preparation and performance optimization were described in our previous research works [37]. The output properties of materials depend to a large extent on the deposition potential and electrolyte composition. The materials used in this work are prepared and selected on the basis of the previous stage. Fig. 3 shows that the microscopic morphology of the annealed n-type and p-type TE materials is extremely dense and uniform and thus suitable for the preparation of RTG devices.

3.2. Output performance of flexible thin-film RTG

The electrical performance test results of the experimentally prepared RTGs are shown in Figs. 4 and 5. Fig. 4 shows the current-voltage-power (I–V–P) curves, and Fig. 5 shows the V_{oc}, short circuit current I_{sc}, temperature difference ΔT, and maximum output power P_{max} of the RTG loaded with different heat source powers. As the current increases, the output voltage of the device gradually drops, and the output power first increases to the peak and then decreases. The peak is the maximum output power P_{max}. For loading heat sources with different powers, the fluctuation range of performance parameters is large, such as I_{sc} = 1.75 μA–7.34 μA, V_{oc} = 38.51 mV–174.88 mV, ΔT = 13.9 K–54.8 K, and P_{max} = 16.06 nW–333.20 nW, respectively. As the heat source power increases, the output performance of the device also increases.

Table 1
Performance of n-type and p-type TE films.

Property	n-type	p-type
Potential (V, vs. Ag/AgCl)	0	−0.12
Seebeck coefficient (μV/K)	−92.166	114.03
Electrical conductivity (S/cm)	956.3	105.49
Power factor (μW/m·K^2)	812.34	137.18
Annealing temperature (°C)	300	250
Thermal conductivity (W/m·K)	3.20	1.03
ZT value (300 K)	0.08	0.03
Chemical formula	$Bi_{1.92}Te_{3.08}$	$Bi_{0.68}Sb_{1.24}Te_{3.08}$

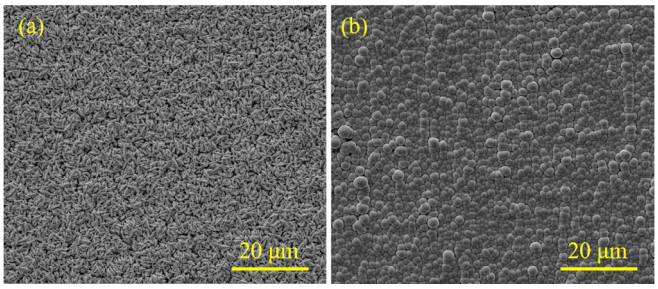

Fig. 3. SEM images of (a) n-type and (b) p-type TE materials after annealing.

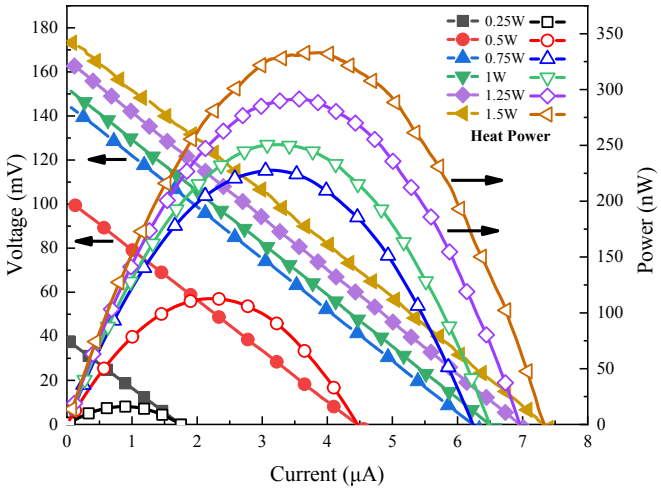

Fig. 4. I–V–P curves of RTG when loading different power heat sources.

The output voltage and power reach maximum values of 174.88 mV and 333.20 nW, respectively, when the device is loaded with a 1.5 W heat source.

3.3. Verification of finite element simulation validity

In the case of TE material determination, in order to obtain better performance output, the multi-physics finite element simulation software (COMSOL Multiphysics) was used to optimize the size parameters and the module number of the fan-shaped RTG. The 3D geometric model of the fan-shaped RTG was established, and the model parameters include certain variables and quantification, which is convenient for later adjustment. The temperature distribution of the RTG at the steady state and the corresponding output performance parameters were extracted and analyzed. The size, shape and material properties of the device during the simulation were as close as possible to the actual situation, and the Seebeck effect, Peltier effect and Joule heat were also considered. All boundaries were set to electrical and thermal insulation during the simulation, and the initial temperature of the device was set at 293.15 K. The device is grounded at one end and its output is the final electrical output of the device under the hot end. In addition, the surface convection heat transfer coefficient is also involved in the simulation process. In general, this value is about 5–25 W/m^2·K in the case of natural convection of the air. In this simulation work we selected 10 W/m^2·K. The regulation heat source power varies from 0.25 to 1.5 W, and the electrical output of the thermoelectric device under different heat source powers is examined. Under the same conditions, the current module of the device can be set to obtain the internal resistance of the device, and the final output

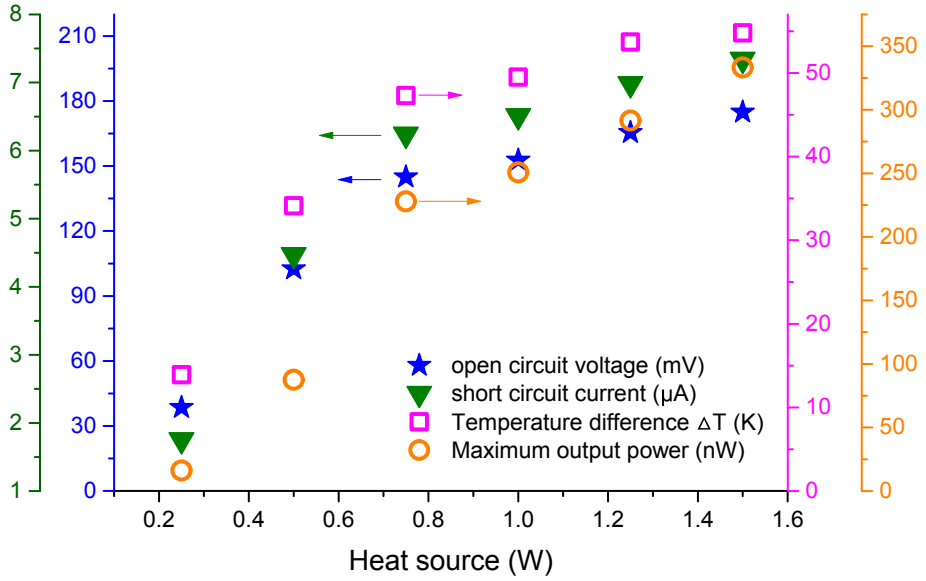

Fig. 5. Output performance of RTG with different power heat sources.

power can be obtained by the obtained voltage and resistance.

The simulation results of the finite element were compared with the experimental results to verify the effectiveness of the COMSOL simulation optimization for RTG. As shown in Fig. 6, the V_{oc}, I_{sc}, ΔT, and P_{out} of the flexible RTG were obtained through experimental testing and software simulation. The output performance of RTG increases gradually with the increase in the power of the loaded heat source, and the trend of the simulation calculation is basically consistent with that of the output performance of the experimentally prepared RTG. The results indicate the feasibility of using the

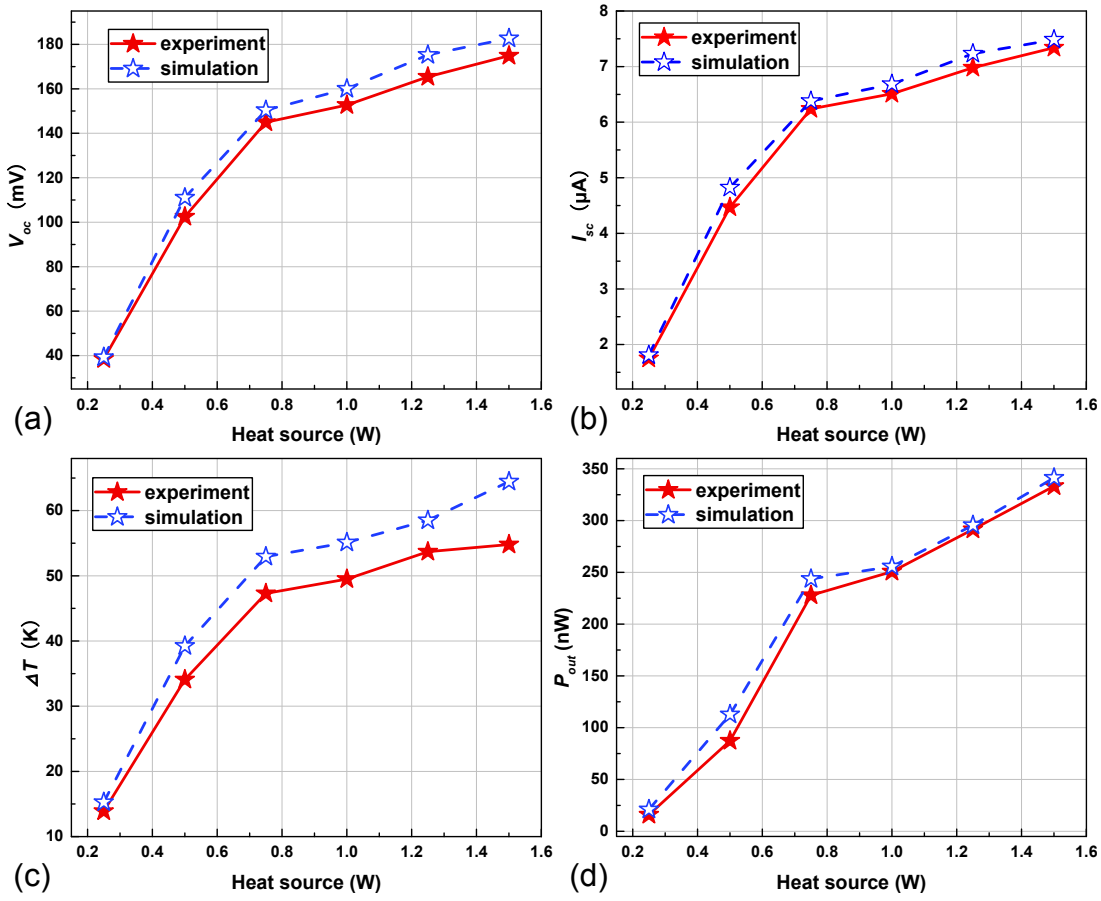

Fig. 6. Comparison of RTG simulation and experimental output performance when loaded with different power heat sources: (a) open circuit voltage, (b) short circuit current, (c) temperature difference, and (d) output power.

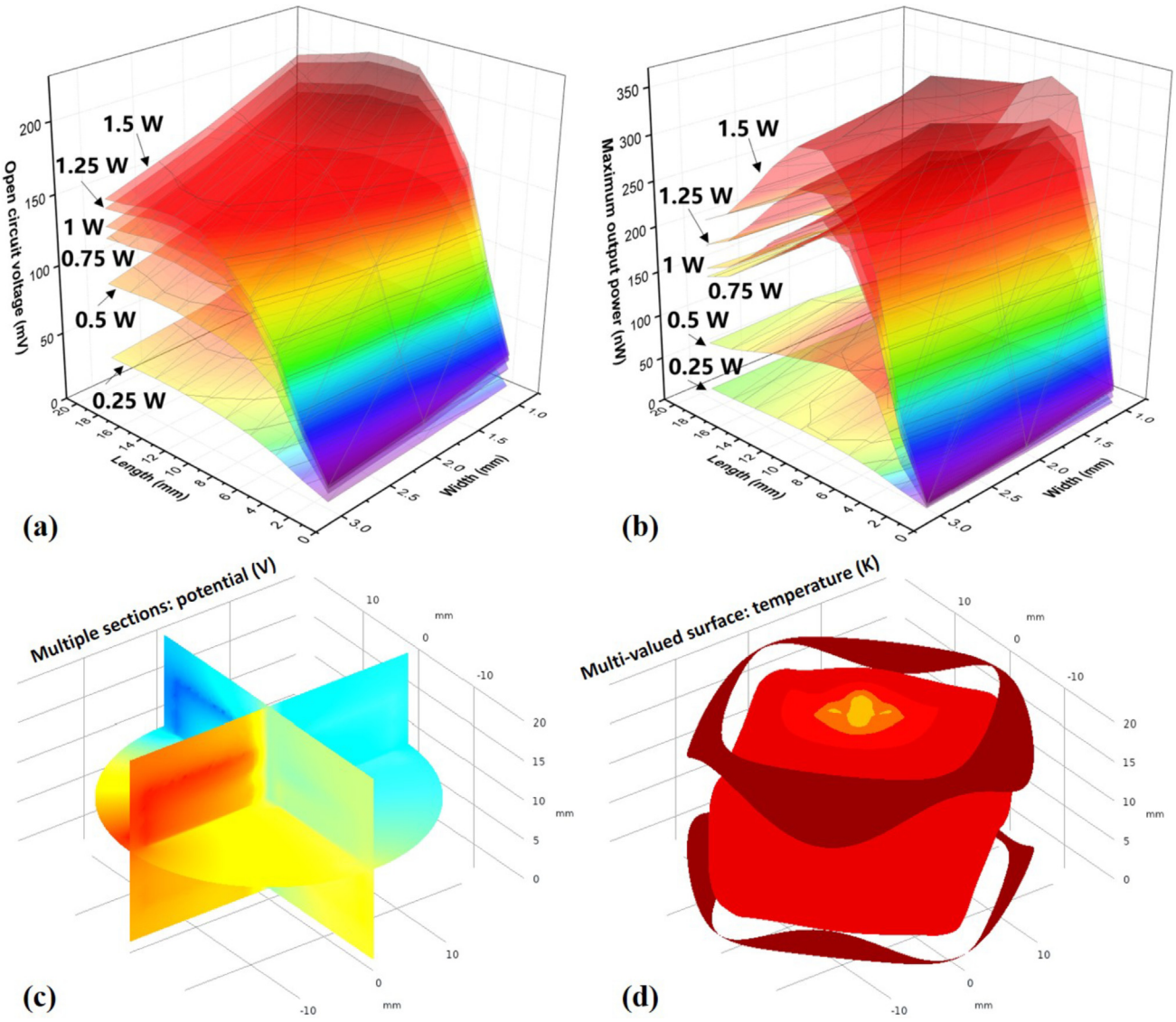

Fig. 7. Output performance of the RTG with different sizes: (a) V_{oc}, (b) P_{max}, (c) potential profile, and (d) temperature profile.

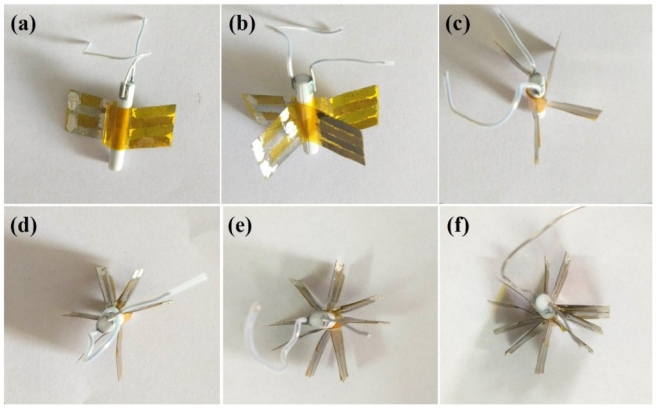

Fig. 8. Photographs of different numbers of TE modules in series: (a) 2, (b) 4 (side view), (c) 4 (top view), (d) 6, (e) 8, and (f) 10.

finite element method for device electrical performance simulation and optimization.

Although the simulated values of the output performance of the RTG are close to the experimental values, the latter is slightly smaller than the former. This finding may be explained by the large contact resistance between the TE leg and the electrode and the limited experimental conditions that may have increased the internal resistance of the RTG. Moreover, the inevitable convective heat transfer environment in the air and the ideality of the simulated environment are also possible causes of this phenomenon.

3.4. Device size optimization

Fig. 7a–b shows the output performance curves of the RTG with different length and width TE leg. Fig. 7c–d reflect the potential distribution diagram and the temperature profile of the device with a TE leg size of 11 × 2 mm^2. In the range of 1–22 mm, as the length of the TE leg increases, the output voltage of the TE device gradually rises to a maximum at a length of 11 mm, and then gradually decreases. As the size of the TE leg increases, the temperature difference across the device also increases, which in turn leads to an

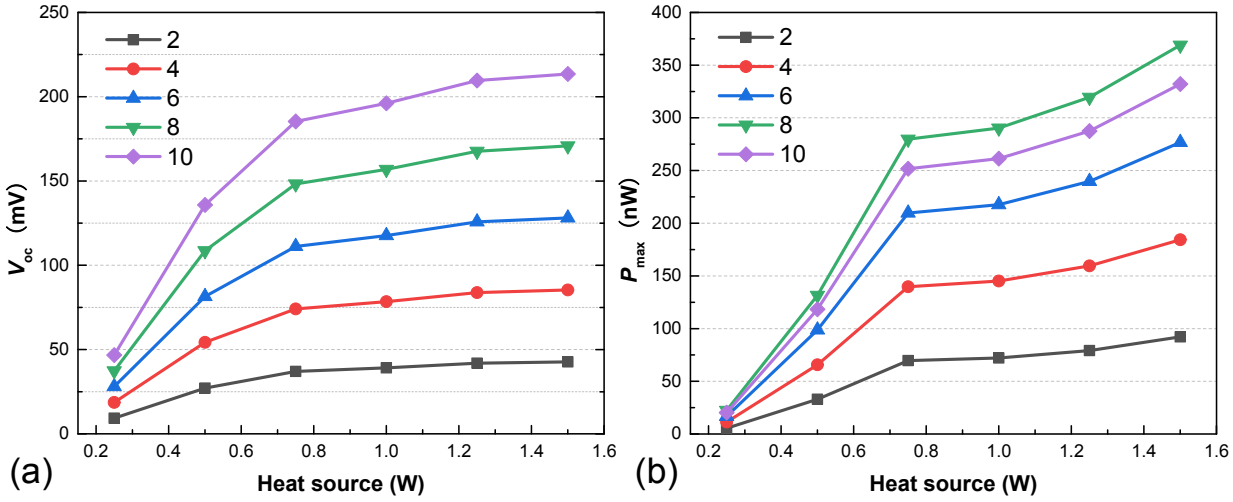

Fig. 9. (a) V_{oc} and (b) P_{max} of RTGs with different TE modules vary with the heat source power.

increase in the output voltage. However, when the length of the TE leg continues to increase, the added polyimide material increases the heat loss, which in turn reduces the temperature difference. Hence, the output voltage has a tendency to decrease in the later stage.

Similarly, when different power sources are loaded, the RTGs with different lengths and widths also have an optimum maximum output power value, as shown in Fig. 7b. The main reason for this phenomenon is that the area of the TE material increases with the length of the TE leg, resulting in an increase in the internal resistance of the RTG and a reduction in the short circuit current. The potential distribution and temperature distribution of the device are shown in Fig. 7c and d. As the heat source power increases, the electrical output performance parameters of the RTG also increase relatively. According to the above analysis results, for this model, when the size of the TE leg is 9×2 mm^2, the V_{oc} and P_{max} reach a maximum value of 170.81 mV and 369.02 nW, respectively. For the actual prepared prototype, the size of the TE leg is 11×2 mm^2, and the corresponding V_{oc} and P_{max} are 182.69 mV and 341.26 nW. Compared with that of the non-optimized size prototype, the output power of the optimized device is increased by 8.13% and has been greatly improved, and the output voltage is slightly reduced by 6.5%. The results show that the simulation optimization can improve the output performance of the device. Although increasing the length of the TE leg can increase the voltage output of the device, the power does not increase infinitely with the length of the TE leg. In practical applications, the device size parameters should be adjusted according to the actual situation.

3.5. Module quantity optimization

Fig. 8 is a photograph of different numbers of TE modules connected in series. Fig. 9 reflects the trend of V_{oc} and P_{max} of the RTG with different numbers of TE modules in the case of loading different power heat sources. Consistent with the simulation results, as the heat source power increases, the electrical performance of the RTG also increases. As the number of TE modules increases, the output voltage and power of the series RTG also gradually increases. When 1.5 W of heat source power is applied, the V_{oc} of the RTG in series with ten TE modules reaches a maximum value of 213.51 mV. The results show that under the same heat source power, the output voltage can be increased by increasing the amount of modules. The variation trend of the output power is slightly different from that of the output voltage. The output power does not increase continuously with the number of TE modules and shows a peak instead. When a 1.5 W heat source is loaded, the RTG with eight TE modules in a series obtains the P_{max} of 369.02 nW. As the number of series modules increases, P_{max} does not increase linearly like V_{oc}, which is primarily due to two reasons. On the one hand, the output power is related to the internal resistance of the device. When the number of series modules increases, the internal resistance of the thin film material also increases continuously, thus reducing the current of the device. On the other hand, the power of the heat source is fixed. When the number of TE modules increases, the input heat of the single TE module decreases and consequently reduces the temperature difference of the device itself.

Fig. 10 compares the experimental and simulated values of the RTG with different numbers of TE modules, with the TE leg size fixed at 9×2 mm^2. As the number of modules increases, the V_{oc} shows a linear increase, while the P_{max} has a peak. For the RTG in this work, when the number of modules goes 8, the output performance of the device is optimal. The calculated V_{oc} and P_{max} is 170.81 mV and 369.02 nW, and the measured V_{oc} and P_{max} is 153.52 mV and 341.44 nW. The calculated value is relatively high, mainly due to the idealized performance of the materials employed in the device during the simulation.

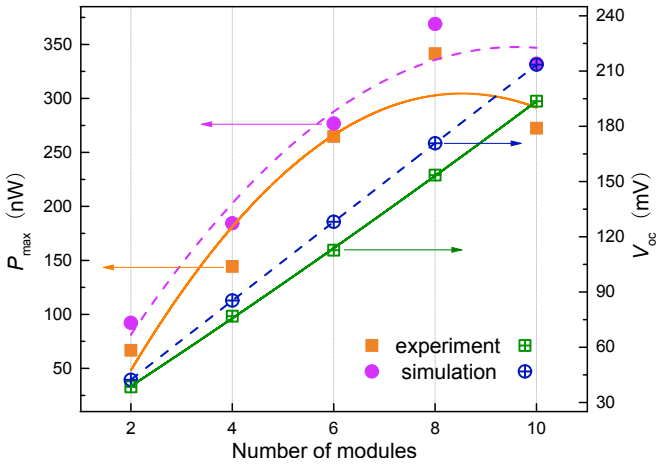

Fig. 10. Comparison of experimental and simulated output performance of RTGs with different module numbers.

4. Conclusions

A fan-shaped miniaturized RTG with 8 TE modules, 32 TE legs, a height of 11 mm, and a diameter of 25.8 mm was designed and fabricated. When the 1.5 W heat source was loaded, the device temperature difference is 54.8 K, the output voltage is 174.88 mV, and the maximum output power is 333.20 nW. The output performance of the sector RTG was tested and optimized. After a series of optimizations on the length and width of the TE leg by the finite element method, the output power of the RTG was increased by 8.13% compared with that in the non-optimized state. Moreover, the series connection of multiple thermoelectric modules can effectively improve the output performance of the device, and the best performance can be achieved by optimizing the structural parameters. Such micro-powered devices can even be widely used in many areas such as deep space exploration and artificial intelligence in the future.

Acknowledgments

The authors acknowledge the support received from the National Natural Science Foundation of China (Grant No. 11675076), China Postdoctoral Science Foundation (Grant No. 2019M661836), the Shanghai Aerospace Science and Technology Innovation Project (Grant No. SAST2016112), and the Fundamental Research Funds for the Central Universities (Grant No. NP2018462).

References

[1] Rowe DM. Applications of nuclear-powered thermoelectric generators in space. Appl Energy 1991;40(4):241–71.
[2] O'Brien RC, Ambrosi RM, Bannister NP, et al. Safe radioisotope thermoelectric generators and heat sources for space applications. J Nucl Mater 2008;377(3):506–21.
[3] Lange RG, Carroll WP. Review of recent advances of radioisotope power systems. Energy Convers Manag 2008;49(3):393–401.
[4] Schmidt GR, Sutliff TJ, Dudzinski LA. Radioisotope power: a key technology for deep space exploration. Radioisotopes-Applications in Physical Sciences. Nirmal Singh. InTech; 2011. p. 419–55.
[5] Tatarinov D, Wallig D, Bastian G. Optimized characterization of thermoelectric generators for automotive application. J Electron Mater 2012;41(6):1706–12.
[6] Champier D. Thermoelectric generators: a review of applications. Energy Convers Manag 2017;140:167–81.
[7] Sutliff TJ, Dudzinski LA, Hamley J, et al. NASA's radioisotope power systems and technologies-a forward look. In: 9th annual international energy conversion engineering conference; 2011. p. 5868.
[8] Shittu S, Li G, Zhao X, et al. Optimized high performance thermoelectric generator with combined segmented and asymmetrical legs under pulsed heat input power. J Power Sources 2019;428:53–66.
[9] Shittu S, Li G, Zhao X, et al. High performance and thermal stress analysis of a segmented annular thermoelectric generator. Energy Convers Manag 2019;184:180–93.
[10] Shittu S, Li G, Akhlaghi YG, et al. Advancements in thermoelectric generators for enhanced hybrid photovoltaic system performance. Renew Sustain Energy Rev 2019;109:24–54.
[11] Ritz F, Peterson CE. Multi-mission radioisotope thermoelectric generator (MMRTG) program overview. 2004 IEEE Aerospace Conference Proceedings (IEEE Cat. No. 04TH8720) 2004;5:2950–7. IEEE.
[12] Bennett G, Lombardo J, Hemler R, et al. Mission of daring: the general-purpose heat source radioisotope thermoelectric generator. In: 4th international energy conversion engineering conference and exhibit (IECEC); 2006. p. 4096.
[13] Prelas MA, Weaver CL, Watermann ML, et al. A review of nuclear batteries. Prog Nucl Energy 2014;75:117–48.
[14] Allen DT, Hiller ND, Bass JC, et al. Fabrication and testing of thermoelectric modules and milliwatt power supplies. AIP Conference. American Institute of Physics; 2004.
[15] Weber J, Potje-Kamloth K, Haase F, et al. Coin-size coiled-up polymer foil thermoelectric power generator for wearable electronics. Sens Actuators A Phys 2006;132(1):325–30.
[16] Whalen SA, Apblett CA, Aselage TL. Improving power density and efficiency of miniature radioisotopic thermoelectric generators. J Power Sources 2008;180(1):657–63.
[17] Gusev VV, Pustovalov AA, Rybkin NN, et al. Milliwatt-power radioisotope thermoelectric generator (RTG) based on plutonium-238. J Electron Mater 2011;40(5):807–11.
[18] Uda K, Seki Y, Saito M, et al. Fabrication of Π-structured Bi-Te thermoelectric micro-device by electrodeposition. Electrochim Acta 2015;153:515–22.
[19] Suarez F, Parekh DP, Ladd C, et al. Flexible thermoelectric generator using bulk legs and liquid metal interconnects for wearable electronics. Appl Energy 2017;202:736–45.
[20] Liu K, Tang XB, Liu YP, et al. High-performance and integrated design of thermoelectric generator based on concentric filament architecture. J Power Sources 2018;393:161–8.
[21] Yuan ZC, Tang XB, Xu ZH, et al. Screen-printed radial structure micro radioisotope thermoelectric generator. Appl Energy 2018;225:746–54.
[22] Wang YC, Shi YG, Mei DQ, et al. Wearable thermoelectric generator to harvest body heat for powering a miniaturized accelerometer. Appl Energy 2018;215:690–8.
[23] Mu EZ, Yang G, Fu XC, et al. Fabrication and characterization of ultrathin thermoelectric device for energy conversion. J Power Sources 2018;394:17–25.
[24] Lee S, Kim K, Kang DH, et al. Vertical silicon nanowire thermoelectric modules with enhanced thermoelectric properties. Nano Lett 2019;19(2):747–55.
[25] Abol-Fotouh D, Dörling B, Zapata-Arteaga O, et al. Farming thermoelectric paper. Energy Environ Sci 2019;12(2):716–26.
[26] Mahmoudinezhad S, Rezania A, Rosendahl LA. Behavior of hybrid concentrated photovoltaic-thermoelectric generator under variable solar radiation. Energy Convers Manag 2018;164:443–52.
[27] Zhou Y, Zhang SM, Xu X, et al. Dynamic piezo-thermoelectric generator for simultaneously harvesting mechanical and thermal energies. Nano Energy 2019:104397.
[28] Chen HP, Huang JG, Zhang H, et al. Experimental investigation of a novel low concentrating photovoltaic/thermal–thermoelectric generator hybrid system. Energy 2019;166:83–95.
[29] Na J, Kim Y, Park T, Park C, Kim E. Preparation of bismuth telluride films with high thermoelectric power factor. ACS Appl Mater Interfaces 2016;8(47):32392–400.
[30] Kim DH, Byon E, Lee GH, et al. Effect of deposition temperature on the structural and thermoelectric properties of bismuth telluride thin films grown by co-sputtering. Thin Solid Films 2006;510(1):148–53.
[31] Venkatasubramanian R, Colpitts T, Watko E, et al. MOCVD of Bi_2Te_3, Sb_2Te_3 and their superlattice structures for thin-film thermoelectric applications. J Cryst Growth 1997;170(1–4):817–21.
[32] Kim JH, Kwon SD, Jeong DY, et al. Structural characteristics of Bi2Te3 and Sb2Te3 films on (001) GaAs substrates grown by MOCVD. International Conference on Thermoelectrics, IEEE; 2006.
[33] Liu S, Hu B, Liu D, et al. Micro-thermoelectric generators based on through glass pillars with high output voltage enabled by large temperature difference. Appl Energy 2018;225:600–10.
[34] Kim J, Lim JH, Myung NV. Composition- and crystallinity-dependent thermoelectric properties of ternary $Bi_xSb_{2-x}Te_y$ films. Appl Surf Sci 2018;429(31):158–63.
[35] Kang WS, Li WJ, Chou WC, et al. Microstructure and thermoelectric properties of Bi_2Te_3 electrodeposits plated in nitric and hydrochloric acid baths. Thin Solid Films 2017;623:90–7.
[36] Trung NH, Toan NV, Ono T. Fabrication of π-type flexible thermoelectric generators using an electrochemical deposition method for thermal energy harvesting applications at room temperature. J Micromech Microeng 2017;27(12):125006.
[37] Li JQ, Tang XB, Liu YP, et al. Fan-shaped flexible radioisotope thermoelectric generators based on Bi_xTe_y and $Bi_xSb_{2-x}Te_y$ fabricated through electrochemical deposition. Energy Technol 2019;7(3):1800707.